Impacts of Wall Materials and Locations on Channel Characteristics and Performance of Indoor Wireless Communication Systems

Xichen Mao, *Graduate Student Member, IEEE*, Cheng-Xiang Wang, *Fellow, IEEE*, Songjiang Yang, *Member, IEEE*, Jingyu Lyu, Jie Huang, *Member, IEEE*, Shuaifei Chen, *Member, IEEE*, and Jie Zhang, *Senior Member, IEEE*

***Abstract*—With over 80% of mobile traffic occurring indoors, optimizing indoor wireless communication performance is crucial. For indoor communication systems, interior walls play a significant role in shaping system performance, yet their impacts on wireless communication performance at the link level remain insufficiently explored. In this paper, we propose an evaluation method for indoor wireless performance, considering wall materials and locations. Based on the evaluation method, the relationships between interior walls and signal propagation are investigated, considering line-of-sight (LOS) probability, blockage height, blockage density, and wall materials. The signal propagations are divided into four cases, including the direct path, the reflection path and/or penetration path through walls, and the multipath from scatterers. Moreover, spatial cross-correlation function (SCCF), spectrum efficiency (SE), and energy efficiency (EE) are analyzed to unveil the impacts of walls on channel characteristics and system performance. Our findings reveal that strategically adjusting the placement and materials of walls, while keeping network settings unchanged, can significantly enhance system performance.**

***Index Terms*—Indoor communications, interior walls, LOS probability, channel characteristics, system performance.**

I. Introduction

INDOOR wireless communications have sparked widespread interests, due to the proliferation of indoor communication users and the dramatic growth of the industrial Internet of things (IIoT) [1]. In the fifth generation (5G) wireless communication systems, indoor communication traffic has already accounted for more than 80% of total traffic in 2022 and the proportion keeps rising [2]. Among the six use cases proposed for the sixth-generation (6G) mobile communication system in [3], indoor systems hold a pivotal role and are highlighted in numerous examples. Hence, improving indoor communication quality is gradually attracting the attention of scholars. Although the multiple-input multiple-output (MIMO) [4], [5] and reconfigurable intelligent surface (RIS) technologies [6] have been adopted in indoor environments to improve the communication system performance, these technologies cannot overcome the limitation of building layouts and blockages in indoor communication environments [7]. The walls, devices, human bodies, and other obstacles have significant influences on signal propagation and system performance.

As obstacles can block the propagation of signals, their influences will be intuitively reflected in path loss. The 3rd generation partnership project (3GPP) proposed the standard to analyze the line-of-sight (LOS) and non-LOS (NLOS) signal path loss for indoor communications [8]. Similarly, international telecommunication union (ITU) also provided different transmission loss calculation methods according to LOS and NLOS signals [9]. Therefore, LOS probability model has become one of the most concerned parameters in indoor communication performance analysis. In [10], ITU presented a calculation method for LOS probability, considering the heights and number of blockages in the propagation link. However, the model did not provide general assessment of LOS probability and needed to be derived specifically with different scenario settings. To obtain a general LOS probability model, it is common to utilize fitting formula [8], [11]. These models based on fitting formula focused on the impacts of propagation distance and ignored the different blockages in different indoor scenarios. To solve the shortcomings of fitting formula, more methods for general LOS probability model were proposed. In [12], a three-dimensional (3D) LOS probability model was proposed, considering the impacts of walls. However, the model was derived based on the empty room, ignoring other blockages. In [13], LOS probability models were proposed for outdoor and indoor systems. The models only considered the impacts of locations of blockages, ignoring the influences of blockage height. In [14], blockage

Received 18 December 2024; revised 27 September 2025; accepted 6 December 2025. Date of publication 23 December 2025; date of current version 12 January 2026. This work was supported in part by the National Natural Science Foundation of China (NSFC) under Grant 62401644 and Grant 62271147; in part by China Post-Doctoral Science Foundation under Grant 2024M752439; in part by the Research Fund of National Mobile Communications Research Laboratory, Southeast University, under Grant 2025A05; and in part by the Program of China Scholarship Council (CSC) under Grant 202406090213. The associate editor coordinating the review of this article and approving it for publication was C. F. Mecklenbräuker. *(Corresponding authors: Cheng-Xiang Wang; Songjiang Yang.)*

Xichen Mao and Jingyu Lyu are with the National Mobile Communications Research Laboratory, School of Information Science and Engineering, Southeast University, Nanjing 211189, China (e-mail: maoxc@seu.edu.cn; lv_jingyu@seu.edu.cn).

Cheng-Xiang Wang, Jie Huang, and Shuaifei Chen are with the National Mobile Communications Research Laboratory, School of Information Science and Engineering, Southeast University, Nanjing 211189, China, and also with the Purple Mountain Laboratories, Nanjing 211111, China (e-mail: chxwang@seu.edu.cn; j_huang@seu.edu.cn; shuaifeichen@seu.edu.cn).

Songjiang Yang is with the Purple Mountain Laboratories, Nanjing 211111, China (e-mail: yangsongjiang@pmlabs.com.cn).

Jie Zhang is with Ranplan Wireless Network Design Ltd., CB23 3UY Cambridge, U.K. (e-mail: jie.zhang@ranplanwireless.com).

Digital Object Identifier 10.1109/TWC.2025.3644391

model for indoor communication systems was derived from LOS probability model. The proposed model was simplified and also ignored the impacts of blockage height. In all, there is a lack of a general LOS probability model considering locations, heights, and density of blockages.

Moreover, the influences of walls on wireless channels have been extensively studied, and are generally categorized into penetration, reflection, diffraction, and scattering. In [15], the impacts of wall material on wall reflection signals were considered in the proposed channel model, but their effects were simplified as constant parameters. In [16], a geometry-based stochastic model (GBSM) was developed for indoor environments, where wall information was embedded into the power-angular-delay profile. Similarly, another GBSM was proposed in [17], in which the angle-delay distribution was derived to analyze the spatial distribution of walls and other scatterers. In [18], the diffraction was considered in channel modeling, but the model mainly focused on the geometric shape rather than other wall characteristics. In [19], a non-stationary channel model for large office environments was proposed and the environment information was analyzed by the measured power data. In [20], a 6G pervasive channel model (6GPCM) was proposed and can be adapted to describe indoor wireless channels. However, this model also used generated ray power to represent impacts of walls. In all, indoor channel models can effectively reveal the correlation between walls and signal propagation. However, wall influences are often embedded into aggregated power or delay distributions, making it difficult to isolate their individual effects. Therefore, it is essential to explicitly extract the impacts of specific wall parameters on signal propagation.

The impacts of walls on communication system performance have also been investigated. In [7], impacts of wall deployment on received signal power were analyzed, but the system model was simplified as two dimensional (2D) systems. In [21], different wall deployment schemes were examined under Rayleigh fading to evaluate communication system performance. The study in [22] investigated wall reflections under Nakagami fading, treating them as a source of power enhancement at the receiver. In [23], impacts of wall structures on signal propagation were presented, while the conclusions were mainly based on simulations. In [24], the relationship between wall deployment and coverage probability was investigated under Rician fading. Impacts of wall materials on signal delays were explored in [25], but the approach heavily depended on detailed and accurate indoor maps. In summary, existing performance evaluations considering walls are often based on simplified channel models which cannot capture the complexity of real propagation environments. Furthermore, current analysis mainly relies on simulations, making it difficult to derive general conclusions. Hence, there is a need for theoretical performance analysis based on more realistic channel models.

To support the theoretical analysis, a novel system performance evaluation framework called building wireless performance (BWP) was proposed in [2]. Within BWP, two new performance metrics, interference gain and power gain, were introduced to quantify impacts of walls on communication performance [26]. In [27], channel capacity was derived considering the reflection. It was shown that when walls are extremely close to transmitters (Tx), the reflection signals can be analyzed in the same way as LOS signals. Based on BWP, impacts of wall penetration on system performance were investigated in [28]. However, existing research usually simplifies wall impacts into a single parameter, overlooking the role of specific wall properties. Therefore, it remains essential to establish relationships between specific wall parameters and system performance.

To solve the above problems, a novel communication performance evaluation method considering wall materials and locations is proposed in this paper. The impacts of walls on LOS probability and signal propagation are investigated. Based on the proposed method, channel characteristics and system performance are analyzed. It is proven that optimizing deployment angle and relative dielectric constant (RDC) of walls can enhance system performance. The main novelties and contributions of this paper are summarized as follows.

1) A novel LOS probability model is developed to characterize the effects of random blockages on signal propagation in indoor environments. The proposed model explicitly incorporates transceiver positions, transceiver density, and blockage heights, making it adaptable to diverse indoor configurations. Moreover, closed-form expressions for LOS probability and corresponding path loss are derived.
2) A new method is proposed to analyze the influence of walls on signal propagation mechanisms, including LOS, penetration, reflection, and scattering. Four representative propagation cases are defined, and for each case, channel characteristics including angles of arrival/departure, delays, channel impulse response, and spatial cross-correlation function (SCCF) are derived with consideration of specific wall parameters. This method can assess the impacts of walls on individual propagation mechanisms.
3) The communication system performance considering wall materials and locations are derived, including spectrum efficiency (SE) and energy efficiency (EE). In particular, SE and EE are expressed in the function of wall parameters such as wall deployment angle and electromagnetic coefficients. Results show that the optimal system performance can be achieved by adjusting wall deployment and wall material selection.

The remainder of the paper is organized as follows. In Section II, the system model for indoor communications is introduced, including the LOS probability model and channel models. Based on the system model, channel characteristics and system performance are discussed in Section III. In Section IV, the results are presented and analyzed. Finally, conclusions are drawn in Section V.

II. System Model

In this section, a novel system model for indoor communication systems is proposed, which considers the impacts of penetration and reflection of walls. With extensive constructions of communication infrastructure, there are various applications and typical indoor communication scenarios, such as industry, library, supermarket, apartment/house, gymnasium, and office. In Fig. 1, the simplified model of indoor

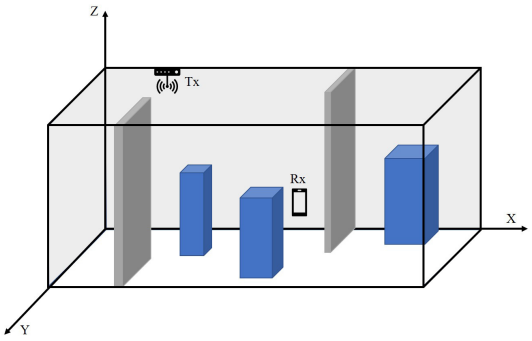

Fig. 1. Illustration of simplified indoor communication scenarios.

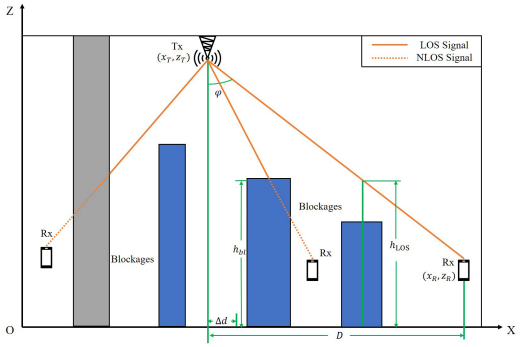

Fig. 2. 2D indoor system model for LOS probability.

communication scenarios is shown. The blue cuboids represent a variety of obstacles, such as devices and furniture. The gray cuboids represent walls. Since cylinders have a rectangular cross-section and curved surfaces have less effect on signal, all blockages are modeled as cuboids for simplicity.

Receivers (Rxs) refer to all ground users and there are many blockages between Tx and Rx. The blockages can be anything inside the building, such as walls, devices, and human. In this paper, it is assumed that Txs are equipped with N_T antennas and Rxs are equipped with N_R antennas. To clearly describe locations of transceivers, the coordinates are (x_R, y_R, z_R) for Rx and (x_T, y_T, z_T) for Tx.

The channel matrix can be expressed as

$$\mathbf{H} = PL^{1/2} \cdot \mathbf{H}_{\mathrm{s}} \tag{1}$$

where PL represents the path loss, $\mathbf{H}_{\mathrm{s}}$ means the channel matrix of small-scale fading. $\mathbf{H}_{\mathrm{s}} = [h_{qp,f_c}(\tau)]_{N_R \times N_T}$ and $h_{qp,f_c}(\tau)$ is the channel impulse response (CIR) between p-th Tx antenna and q-th Rx antenna.

A. LOS Probability and Path Loss

In this paper, the indoor propagation environment is assumed to be isotropic, which means that the azimuth angle of departure has no impact on the LOS probability. Hence, the 3D system can be simplified to be 2D and the system is illustrated in Fig. 2. It is assumed that the coordinates of Tx and Rx in 2D model are (x_T, z_T) and (x_R, z_R), respectively. The elevation angle of the signal is represented by φ. The projection distance of Tx and Rx on the X-Y plane is expressed as D. The height of one blockage is h_{bl} and the height of the LOS signal at the corresponding location is h_{LOS}. The only situation where LOS signal can be obtained is that at any obstacle, $h_{bl} < h_{\mathrm{LOS}}$.

In the real indoor system, blockages are individual objects, such as walls and equipment, randomly distributing throughout a room. Since the blockages are discrete, it is reasonable to simplify the continuous signal propagation process to a discrete process. The projection distance D can be divided into several N discrete points with a small interval Δd. Then, the set of distances between Tx and discrete points can be represented as $\left\{X(n) \mid X(n) = n\Delta d, n = 0, 1, \ldots, \frac{D}{\Delta d}\right\}$. At the n-th point, the LOS probability can be represented by $P\{X(n) \mid X(0), X(1), \ldots, X(n-1)\}$. The expression means the state of n-th point depends on the states of the previous points. However, as the blockages are independently distributed, the LOS probability at n-th point only depends on the blockages between the $(n-1)$-th and n-th points. Hence, the LOS probability at the n-th point can be derived as

$$P\{X(n) \mid X(0), \ldots, X(n-1)\} = P\{X(n) \mid X(n-1)\}. \tag{2}$$

Therefore, the LOS probability model can be analyzed using a discrete Markov process. The expression of (2) can be simplified as $P_{\mathrm{LOS},n}$. At each point, there are two signal states, i.e., LOS and NLOS signal. Then, the state transition function from n-th to $(n+1)$-th point is

$$\mathbf{P} = \begin{bmatrix} P_{\mathrm{LOS},n} & 1 - P_{\mathrm{LOS},n} \\ 0 & 1 \end{bmatrix} \tag{3}$$

where the first row indicates that $X(n)$ is a LOS signal, the second row indicates that $X(n)$ is a NLOS signal, the first column indicates that $X(n+1)$ is a LOS signal, and the second column indicates that $X(n+1)$ is a NLOS signal. As the state transition function depends on the location of the point, LOS probability is a non-homogeneous discrete Markov process. It is assumed that the distance between Tx and n-th point is d. The LOS probability at the next point $(d + \Delta d)$ is

$$P(d + \Delta d) = P(d) P_{\mathrm{LOS},n} \tag{4}$$

where $P(d)$ and $P(d + \Delta d)$ mean the LOS probability.

Since the presence or absence of an obstacle is unknown for the next position, a Poisson process is introduced to characterize the probability of the presence of an obstacle [29]. Due to the isotropic propagation environment, the number of blockages in the unit distance is assumed to be λ and the probability of an obstacle existing within the distance Δd can be calculated as $P_e = \lambda \Delta d$. Then, the LOS probability can be further derived as

$$P(d + \Delta d) = P(d)[(1 - P_e) + P\{h_{bl} < h_{\mathrm{LOS}}\} P_e] \tag{5}$$

where $P\{h_{bl} < h_{\mathrm{LOS}}\}$ means the probability that the obstacle cannot block the LOS signal and the notation will be simplified as P_h later. Then the LOS probability can be obtained by

$$\frac{1}{P(d)} \frac{P(d + \Delta d) - P(d)}{\Delta d} = P_h \lambda - \lambda. \tag{6}$$

Based on (6), the derivation of $\ln(P(D))$ can be obtained and $P(D)$ is the LOS probability function. Rayleigh distribution is one of the most common distributions of blocking heights and is used in the derivation of the ITU LOS probability models [10]. The probability density function of the blockage height based on Rayleigh distribution is

$$f(h_{bl}) = \frac{h_{bl}}{\sigma^2} \exp\left(-\frac{{h_{bl}}^2}{2\sigma^2}\right) \tag{7}$$

where σ is the Rayleigh distribution scale parameter. Then, P_h can be expressed as $P_h = 1-\exp\left(-\frac{h_{\text{LOS}}^2}{2\sigma^2}\right)$ where $h_{\text{LOS}} = z_T - \frac{D}{\tan\varphi}$. Then the LOS probability model in natural logarithmic form can be obtained by (8), as shown at the bottom of the page. In (8), $\tan\varphi = \frac{D}{Z_T - Z_R}$ and erf$(\cdot)$ means Gauss error function. The LOS probability is $P(D) = \exp\{\ln[P(D)]\}$.

Based on the LOS probability model, the average path loss for the single link can be derived. For the LOS signal, the path loss can be modeled as the free space propagation and the expression is

$$PL_{\text{LOS}}(D) = 10\log_{10}\left(\frac{4\pi f_c}{c}\right)^2 + 10n_L\log_{10}\left(\frac{D}{\sin\varphi}\right) \quad (9)$$

where f_c means the carrier frequency, c represents the speed of light, and n_L is the path loss factor. For the indoor scenario, the common value of n_L tends to be 1.6-1.8. The path loss for NLOS signal is

$$PL_{\text{NLOS}}(D) = 10\log_{10}\left(\frac{4\pi f_c}{c}\right)^2 + 10n_N\log_{10}\left(\frac{D}{\sin\varphi}\right) + D\lambda PL_{\text{bl}} \quad (10)$$

where PL_{bl} means the penetration loss of the blockages and n_N is the path loss factor. The common value of n_N tends to be 2-4. In this paper, the blockages are assumed to be iron. Considering the LOS probability, the average path loss with the projection distance is

$$PL(D) = P(D)\,PL_{\text{LOS}}(D) + (1 - P(D))\,PL_{\text{NLOS}}(D). \quad (11)$$

Based on the average path loss, the impacts of all indoor blockages on signal propagation can be represented.

B. Small-Scale Fading

In complex indoor environments, scattering is almost always present, while LOS, penetration, and reflection occur conditionally depending on the relative positions of blockages and transceivers [15]. In this paper, penetration and reflection are assumed to be primarily caused by walls, whereas scatterers consist of walls, devices, and furniture. When walls are treated as scatterers, wall characteristics can be neglected [27].

The signal propagation is classified into four cases, i.e., signal propagation without penetration and reflection, with penetration and without reflection, with reflection and without penetration, and with penetration and reflection. Specifically, Case 1 corresponds to the condition where no walls block the LOS path or are in very close proximity to Txs. The received signal consists of the LOS component and multipath components from surrounding clusters. Case 2 describes the scenario in which the LOS path is obstructed by the wall and the received signal consists of the penetration component along with multipath signals. Case 3 represents the scenario where the Tx is mounted on a wall, thereby generating a strong reflection component. According to [27], this reflection is comparable in strength and stability to the LOS path and can be further influenced by wall material properties. Therefore, the received signal in Case 3 includes LOS, reflection, and multipath components. Case 4 extends Case 3 by introducing a blocking wall between Tx and Rx, such that the LOS component is removed. The received signal in this case consists of the penetration, reflection, and multipath components. To make it clear, the descriptions and illustrations of four cases are shown in Table I.

1) Case 1: Without Penetration and Reflection: In this case, since there is no penetration or wall reflection, the CIR can adopt the expressions in [20], shown as

$$h_{qp,f_c}(\tau) = \varepsilon_1 h_{qp,f_c}^{\text{LOS}}(\tau) + \varepsilon_3 h_{qp,f_c}^{\text{NLOS}}(\tau) \quad (12)$$

where τ means the delay, and ε_1 and ε_3 represent the power ratio between the two components, i.e., $\varepsilon_1 = \sqrt{\frac{\left|h_{qp,f_c}^{\text{LOS}}(\tau)\right|^2}{\left|h_{qp,f_c}^{\text{LOS}}(\tau)\right|^2 + \left|h_{qp,f_c}^{\text{NLOS}}(\tau)\right|^2}}$ and $\varepsilon_3 = \sqrt{1-\varepsilon_1^2}$. The details of $h_{qp,f_c}^{\text{LOS}}(\tau)$ and $h_{qp,f_c}^{\text{NLOS}}(\tau)$ are shown in (13) and (14), at the bottom of the page, where $[\cdot]^T$ represents the transposition, $F_{q/p,f_c,\text{V/H}}$ represents the antenna patterns of Rx/Tx antenna for vertical/horizontal polarizations, κ_{m_n} is the cross polarization power ratio, μ is co-polar imbalance, $\theta_{mn}^{\text{VV/VH/HV/HH}}$ and $\theta_{\text{L}}^{\text{VV/HH}}$ are initial phases which are uniformly distributed over $(0, 2\pi]$, N_{qp} is the number of clusters, M_n is the number of rays following Poisson distributions in n-th cluster, P_{qp,m_n,f_c} is the power of the ray, τ_{qp}^{L} and τ_{qp,m_n} are the delay, $\phi_{A/E,\text{L}}^{\text{R/T}}$ means the azimuth/elevation angle of Rx/Tx for LOS signal, and $\phi_{A/E,m_n}^{\text{R/T}}$ means the azimuth/elevation angle of Rx/Tx for other multipath signals.

Assume that the coordinate of the n-th cluster is $(x_{m_n}, y_{m_n}, z_{m_n})$. The elevation angles of arrival and departure

$$\ln[P(D)] = \int_0^D P_h\lambda - \lambda\,dd = -\lambda\int_0^D \exp\left(-\frac{\left(z_T - \frac{d}{\tan\varphi}\right)^2}{2\sigma^2}\right)dd = \sqrt{2}\sigma\lambda\tan\varphi\left[\text{erf}\left(\frac{z_T\tan\varphi - D}{\tan\varphi\sqrt{2}\sigma}\right) - \text{erf}\left(\frac{z_T}{\sqrt{2}\sigma}\right)\right]. \quad (8)$$

$$h_{qp,f_c}^{\text{LOS}}(\tau) = \begin{bmatrix} F_{q,f_c,V}\left(\phi_{E,\text{L}}^{\text{R}},\phi_{A,\text{L}}^{\text{R}}\right) \\ F_{q,f_c,H}\left(\phi_{E,\text{L}}^{\text{R}},\phi_{A,\text{L}}^{\text{R}}\right)\end{bmatrix}^T \begin{bmatrix} e^{j\theta_{\text{L}}^{\text{VV}}} & 0 \\ 0 & e^{j\theta_{\text{L}}^{\text{HH}}}\end{bmatrix} \begin{bmatrix} F_{p,f_c,V}\left(\phi_{E,\text{L}}^{\text{T}},\phi_{A,\text{L}}^{\text{T}}\right) \\ F_{p,f_c,H}\left(\phi_{E,\text{L}}^{\text{T}},\phi_{A,\text{L}}^{\text{T}}\right)\end{bmatrix} \cdot e^{j2\pi f_c\tau_{qp}^{\text{L}}}\delta\left(\tau - \tau_{qp}^{\text{L}}\right) \quad (13)$$

$$h_{qp,f_c}^{\text{NLOS}}(\tau) = \sum_{n=1}^{N_{qp}}\sum_{m_n=1}^{M_n} \begin{bmatrix} F_{q,f_c,V}\left(\phi_{E,m_n}^{\text{R}},\phi_{A,m_n}^{\text{R}}\right) \\ F_{q,f_c,H}\left(\phi_{E,m_n}^{\text{R}},\phi_{A,m_n}^{\text{R}}\right)\end{bmatrix}^T \begin{bmatrix} e^{j\theta_{mn}^{\text{VV}}}\sqrt{\mu\kappa_{m_n}^{-1}}e^{j\theta_{m_n}^{\text{VH}}} \\ \sqrt{\kappa_{m_n}^{-1}}e^{j\theta_{m_n}^{\text{HV}}}\sqrt{\mu}e^{j\theta_{m_n}^{\text{HH}}}\end{bmatrix} \begin{bmatrix} F_{p,f_c,V}\left(\phi_{E,m_n}^{\text{T}},\phi_{A,m_n}^{\text{T}}\right) \\ F_{p,f_c,H}\left(\phi_{E,m_n}^{\text{T}},\phi_{A,m_n}^{\text{T}}\right)\end{bmatrix} \cdot\sqrt{P_{qp,m_n,f_c}}\cdot e^{j2\pi f_c\tau_{qp,m_n}}\cdot\delta\left(\tau - \tau_{qp,m_n}\right). \quad (14)$$

TABLE I
DESCRIPTIONS AND ILLUSTRATIONS OF FOUR SIGNAL PROPAGATION CASES

Case	Description	Received Signal	Typical Scenario	Illustration
Case 1: Without penetration and reflection	No wall blocks the LOS path, and no wall is close enough to Tx to cause strong reflection.	LOS signal, multipath signal	Tx and Rx are in the same open area with minimal wall interference.	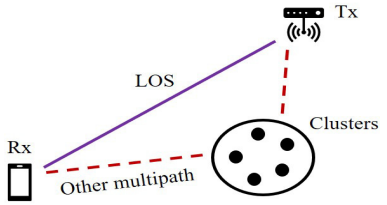
Case 2: With penetration, without reflection	The LOS path is blocked by a wall, while no wall is close enough to Tx.	Penetration signal, multipath signal	Tx and Rx are in adjacent space separated by a wall.	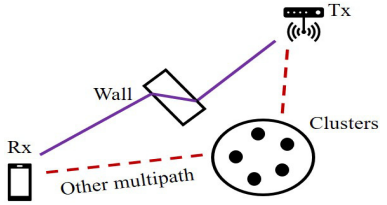
Case 3: With reflection, without penetration	No wall blocks the LOS path, but the Tx is deployed in close proximity to or on a wall, producing a strong reflection signal.	LOS signal, reflection signal, multipath signal	Tx and Rx are in the same open area while Tx is mounted on a wall.	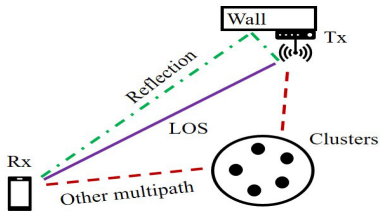
Case 4: With penetration and reflection	The LOS link is blocked by a wall and the Tx is deployed in close proximity to or on another wall.	Penetration signal, reflection signal, multipath signal	Tx is mounted on a wall and separated from Rx by another wall.	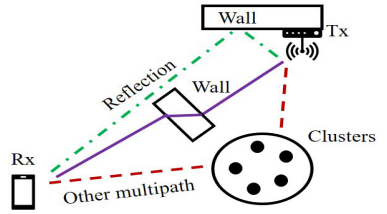

are

$$\begin{aligned}
\phi_{E,\mathrm{L}}^{\mathrm{R}} &= \arctan\frac{|z_T - z_R|}{\sqrt{(x_T - x_R)^2 + (y_T - y_R)^2}} \\
\phi_{E,m_n}^{\mathrm{R}} &= \arctan\frac{|z_{m_n} - z_R|}{\sqrt{(x_{m_n} - x_R)^2 + (y_{m_n} - y_R)^2}} \\
\phi_{E,\mathrm{L}}^{\mathrm{T}} &= \arctan\frac{\sqrt{(x_T - x_R)^2 + (y_T - y_R)^2}}{|z_T - z_R|} \\
\phi_{E,m_n}^{\mathrm{T}} &= \arctan\frac{\sqrt{(x_T - x_{m_n})^2 + (y_T - y_{m_n})^2}}{|z_T - z_{m_n}|}.
\end{aligned} \tag{15}$$

The azimuth angles of arrival and departure are

$$\begin{aligned}
\phi_{A,\mathrm{L}}^{\mathrm{R}} &= \arctan\frac{|y_T - y_R|}{|x_T - x_R|} \\
\phi_{A,m_n}^{\mathrm{R}} &= \arctan\frac{|y_{m_n} - y_R|}{|x_{m_n} - x_R|} \\
\phi_{A,\mathrm{L}}^{\mathrm{T}} &= \arctan\frac{|x_T - x_R|}{|y_T - y_R|} \\
\phi_{A,m_n}^{\mathrm{T}} &= \arctan\frac{|x_T - x_{m_n}|}{|y_T - y_{m_n}|}.
\end{aligned} \tag{16}$$

To simplify the system model, it is assumed that all antennas are omnidirectional and the expressions for $h_{qp,f_c}^{\mathrm{LOS}}(\tau)$ and $h_{qp,f_c}^{\mathrm{NLOS}}(\tau)$ can be

$$h_{qp,f_c}^{\mathrm{LOS}}(\tau) = e^{j2\pi f_c \tau_{qp}^{\mathrm{L}}} \delta\left(\tau - \tau_{qp}^{\mathrm{L}}\right) \tag{17}$$

$$h_{qp,f_c}^{\mathrm{NLOS}}(\tau) = \sum_{n=1}^{N_{qp}} \sum_{m_n=1}^{M_n} \sqrt{P_{qp,m_n,f_c}} \cdot e^{j2\pi f_c \tau_{qp,m_n}} \cdot \delta\left(\tau - \tau_{qp,m_n}\right). \tag{18}$$

The delays are expressed as

$$\tau_{qp}^{\mathrm{L}} = \frac{\sqrt{(x_T - x_R)^2 + (y_T - y_R)^2 + (z_T - z_R)^2}}{c} \tag{19}$$

$$\tau_{qp,m_n}^{\mathrm{L}} = \frac{\sqrt{(x_T - x_{m_n})^2 + (y_T - y_{m_n})^2 + (z_T - z_{m_n})^2}}{c} + \frac{\sqrt{(x_{m_n} - x_R)^2 + (y_{m_n} - y_R)^2 + (z_{m_n} - z_R)^2}}{c}. \tag{20}$$

2) Case 2: With Penetration and Without Reflection: In this case, the signal penetrates the wall and the propagation path is shifted. To explain it clearly, the 3D propagation needs to be

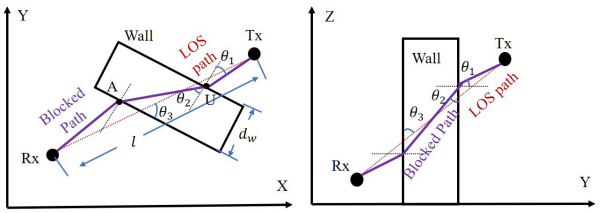

Fig. 3. Penetration path in X-Y and Y-Z planes.

divided into X-Y and Y-Z planes. The shifted paths are shown in Fig. 3.

To simplify the model, it is assumed that the thickness of walls is the same and can be denoted as d_w. The function of the direct link between Rx and Tx can be denoted as $\frac{y-y_R}{x-x_R} = \frac{y_T-y_R}{x_T-x_R}$. As the boundaries of walls are parallel, the two boundaries can be expressed as $y = k_1 x + b_{1/2}$ and $b_{1/2}$ denotes the difference between the two boundaries. Then, the intersection angle of LOS links and walls can be calculated by $\theta_3 = \arctan\left(\left|\frac{k_1-\frac{y_T-y_R}{x_T-x_R}}{1+\frac{y_T-y_R}{x_T-x_R}k_1}\right|\right)$ and $|\cdot|$ denotes absolute value. The straight-line distance between Rx and Tx is $l = \sqrt{(x_T-x_R)^2+(y_T-y_R)^2}$. According to Snell's law, the relationship between θ_1 and θ_2 is $\sin\theta_1 = a\sin\theta_2$ and $a = \eta_2/\eta_1$, where $\eta_{1/2}$ is the refractive index of the different materials. As the LOS link is blocked by a wall, the azimuth angle of arrival/departure and the propagation delay will be different due to refraction.

Lemma 1: The distance of penetration path is

$$\mathrm{AU} = \sqrt{\left(\frac{-\xi_2+\mathrm{sgn}\left(\mathcal{E}\right)\sqrt{\frac{\mathcal{D}+\mathcal{G}}{3}}-\sqrt{\frac{2\mathcal{D}-\mathcal{G}+2\sqrt{\mathcal{Z}}}{3}}}{4\xi_1}\right)^2+d_w^2}. \tag{21}$$

Proof: The detailed proof and explanation of notations are shown in Appendix.■

Based on the derivation of AU, the incident angle and refractive angle can be obtained by $\theta_1 = \arcsin\frac{a\sqrt{\mathrm{AU}^2-d_w^2}}{\mathrm{AU}}$ and $\theta_2 = \arccos\frac{d_w}{\mathrm{AU}}$, respectively. Then, the real propagation distance is obtained by

$$l'_{X-Y} = \mathrm{AU}\left(1+\frac{\cos\left(\theta_2+\theta_3\right)}{\cos\left(\theta_1+\theta_3\right)}\right). \tag{22}$$

The azimuth angle of arrival and departure can be obtained by $\phi^{\mathrm{R}}_{A,\mathrm{B}} = \arctan\frac{|y_T-y_R|}{|x_T-x_R|}+\frac{\pi}{2}-\theta_1-\theta_3$ and $\phi^{\mathrm{T}}_{A,\mathrm{B}} = \arctan\frac{|x_T-x_R|}{|y_T-y_R|}+\theta_1+\theta_3-\frac{\pi}{2}$, respectively.

In this paper, all the walls are assumed to be perpendicular to the floor. Hence, the propagation in Y-Z plane can be calculated similarly to the X-Y plane, but the expressions of walls' boundaries can be simplified as $y = b_{1/2}$. Then the propagation distance l'_{Y-Z} can be obtained similar to (22) and the elevation angle of arrival and departure can be obtained by $\phi^{R}_{E,\mathrm{B}} = \arctan\frac{|y_T-y_R|}{|x_T-x_R|}+\theta_1+\theta_3-\frac{\pi}{2}$ and $\phi^{T}_{E,\mathrm{B}} = \arctan\frac{|x_T-x_R|}{|y_T-y_R|}+\frac{\pi}{2}-\theta_1-\theta_3$, respectively. Moreover, the delay can be obtained by

$$\tau^{\mathrm{B}}_{qp} = \frac{\sqrt{l'^2_{X-Y}+l'^2_{Y-Z}}}{c}. \tag{23}$$

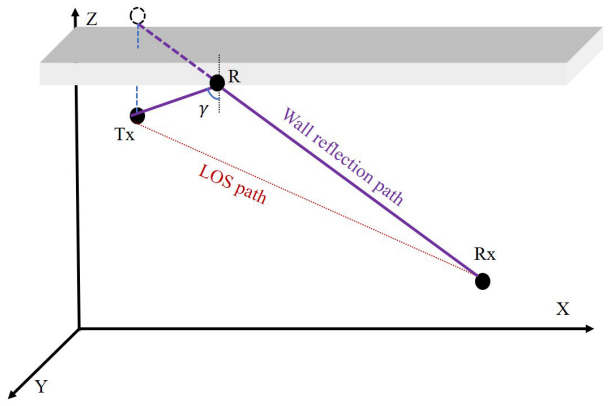

Fig. 4. Illustration of the reflection path.

When signal penetrates the walls, the signal suffers not only from the path loss but also the penetration loss. The penetration loss can be evaluated by the penetration coefficient T. The electronic waves can be divided into transverse electric (TE) polarization and transverse magnetic (TM) polarization. Then the penetration coefficient needs to be calculated by TE and TM polarization. The coefficients for TE and TM waves [30] are expressed as

$$T_{\mathrm{TE}} = \frac{2\cos\theta_1}{\cos\theta_1+\sqrt{\varepsilon-\sin^2\theta_1}} \tag{24}$$

$$T_{\mathrm{TM}} = \frac{2\sqrt{\varepsilon}\cos\theta_1}{\varepsilon\cos\theta_1+\sqrt{\varepsilon-\sin^2\theta_1}} \tag{25}$$

where θ_1 means the incident angle and is illustrated in Fig. 3. Then the penetration coefficient can be obtained by $T = \sqrt{\left(T_{\mathrm{TE}}{}^2+T_{\mathrm{TM}}{}^2\right)/2}$. The CIR for this case is

$$h_{qp,f_c}(\tau) = \varepsilon_1 h^{\mathrm{B}}_{qp,f_c}(\tau)+\varepsilon_3 h^{\mathrm{NLOS}}_{qp,f_c}(\tau) \tag{26}$$

$$h^{\mathrm{B}}_{qp,f_c}(\tau) = \sqrt{T}e^{j2\pi f_c\tau^{\mathrm{B}}_{qp}}\delta\left(\tau-\tau^{\mathrm{B}}_{qp}\right) \tag{27}$$

where $\varepsilon_1 = \sqrt{\frac{\left|h^{\mathrm{B}}_{qp,f_c}(\tau)\right|^2}{\left|h^{\mathrm{B}}_{qp,f_c}(\tau)\right|^2+\left|h^{\mathrm{NLOS}}_{qp,f_c}(\tau)\right|^2}}$. The other components in (27) are similar to (12).

3) Case 3: With Reflection and Without Penetration: In this case, the reflection is caused by walls and the reflection path is shown in Fig. 4. Without loss of generality, it is assumed that the function of the wall can be expressed as $k_2x+k_3y+k_4z+k_5 = 0$. According to the geometric relationship, the coordinate of the symmetric point of Rx is $x_{us} = \frac{k_3^2x_R+k_4^2x_R-k_2^2x_R-k_2k_3y_R-k_2k_4z_R-k_2k_5}{k_2^2+k_3^2+k_4^2}$, $y_{us} = \frac{k_2^2y_R+k_4^2y_R-k_3^2y_R-k_2k_3x_R-k_3k_4z_R-k_3k_5}{k_2^2+k_3^2+k_4^2}$, and $z_{us} = \frac{k_2^2z_R+k_3^2z_R-k_4^2z_R-k_2k_4x_R-k_3k_4y_R-k_4k_5}{k_2^2+k_3^2+k_4^2}$. Furthermore, the coordinate of the reflection point can be derived as $x_{wr} = x_T+(x_{us}-x_T)m_{rf}$, $y_{wr} = y_T+(y_{us}-y_T)m_{rf}$, and $z_{wr} = z_T+(z_{us}-z_T)m_{rf}$, where $m_{rf} = -\frac{k_2x_T+k_3y_T+k_4z_T+k_5}{k_2(x_{us}-x_T)+k_3(y_{us}-y_T)+k_4(z_{us}-z_T)}$. The delay of the reflection can be calculated by

$$\tau^{\mathrm{WR}}_{qp} = \frac{\sqrt{(x_T-x_{wr})^2+(y_T-y_{wr})^2+(z_T-z_{wr})^2}}{c}$$

$$+\frac{\sqrt{(x_{wr}-x_R)^2+(y_{wr}-y_R)^2+(z_{wr}-z_R)^2}}{c}. \tag{28}$$

Similar to the penetration, the signal also suffers from reflection loss which is evaluated by the reflection coefficient. The reflection coefficients for TE and TM waves [30] are

$$\Gamma_{\mathrm{TE}}=\frac{\cos\gamma-\sqrt{\varepsilon-\sin^2\gamma}}{\cos\gamma+\sqrt{\varepsilon-\sin^2\gamma}} \tag{29}$$

$$\Gamma_{\mathrm{TM}}=\frac{\varepsilon\cos\gamma-\sqrt{\varepsilon-\sin^2\gamma}}{\varepsilon\cos\gamma+\sqrt{\varepsilon-\sin^2\gamma}} \tag{30}$$

where γ is incident angle and can be obtained by $\gamma=\arccos\sqrt{\frac{(y_T-y_{wr})^2+(z_T-z_{wr})^2}{(x_T-x_{wr})^2+(y_T-y_{wr})^2+(z_T-z_{wr})^2}}$. Then, the reflection coefficient can be expressed as $\Gamma=\sqrt{\left(\Gamma_{\mathrm{TE}}{}^2+\Gamma_{\mathrm{TM}}{}^2\right)/2}$.

Hence, the CIR for this case can be expressed as

$$h_{qp,f_c}(\tau)=\varepsilon_1 h^{\mathrm{LOS}}_{qp,f_c}(\tau)+\varepsilon_2 h^{\mathrm{WR}}_{qp,f_c}(\tau)+\varepsilon_3 h^{\mathrm{NLOS}}_{qp,f_c}(\tau) \tag{31}$$

where $h^{\mathrm{WR}}_{qp,f_c}(\tau)$ represents the channel matrix of small scale fading for the reflection signal and the expressions of $h^{\mathrm{LOS}}_{qp,f_c}(\tau)$ and $h^{\mathrm{NLOS}}_{qp,f_c}(\tau)$ are the same to (12). Moreover, the expressions for the power ratio are $\varepsilon_1=\sqrt{\frac{\left|h^{\mathrm{LOS}}_{qp,f_c}(\tau)\right|^2}{\left|h^{\mathrm{LOS}}_{qp,f_c}(\tau)\right|^2+\left|h^{\mathrm{WR}}_{qp,f_c}(\tau)\right|^2+\left|h^{\mathrm{NLOS}}_{qp,f_c}(\tau)\right|^2}}$, $\varepsilon_2=\sqrt{\frac{\left|h^{\mathrm{WR}}_{qp,f_c}(\tau)\right|^2}{\left|h^{\mathrm{LOS}}_{qp,f_c}(\tau)\right|^2+\left|h^{\mathrm{WR}}_{qp,f_c}(\tau)\right|^2+\left|h^{\mathrm{NLOS}}_{qp,f_c}(\tau)\right|^2}}$, and $\varepsilon_3=\sqrt{\frac{\left|h^{\mathrm{NLOS}}_{qp,f_c}(\tau)\right|^2}{\left|h^{\mathrm{LOS}}_{qp,f_c}(\tau)\right|^2+\left|h^{\mathrm{WR}}_{qp,f_c}(\tau)\right|^2+\left|h^{\mathrm{NLOS}}_{qp,f_c}(\tau)\right|^2}}$. Based on the geometric relationship, the expression of $h^{\mathrm{WR}}_{qp,f_c}(\tau)$ is

$$h^{\mathrm{WR}}_{qp,f_c}(\tau)=\sqrt{\Gamma}e^{j2\pi f_c\tau^{\mathrm{WR}}_{qp}}\delta\left(\tau-\tau^{\mathrm{WR}}_{qp}\right). \tag{32}$$

The corresponding azimuth and elevation angles are $\phi^{\mathrm{R}}_{E,\mathrm{WR}}=\arctan\frac{|z_{wr}-z_R|}{\sqrt{(x_{wr}-x_R)^2+(y_{wr}-y_R)^2}}$, $\phi^{\mathrm{T}}_{E,\mathrm{WR}}=\arctan\frac{\sqrt{(x_T-x_{wr})^2+(y_T-y_{wr})^2}}{|z_T-z_{wr}|}$, $\phi^{\mathrm{R}}_{A,\mathrm{WR}}=\arctan\frac{|y_{wr}-y_R|}{|x_{wr}-x_R|}$, and $\phi^{\mathrm{T}}_{A,\mathrm{WR}}=\arctan\frac{|x_T-x_{wr}|}{|y_T-y_{wr}|}$.

4) Case 4: With Penetration and Reflection: In this case, the LOS signal is blocked by a wall and there is a wall in close proximity to Tx. The CIR is

$$h_{qp,f_c}(\tau)=\varepsilon_1 h^{\mathrm{B}}_{qp,f_c}(\tau)+\varepsilon_2 h^{\mathrm{WR}}_{qp,f_c}(\tau)+\varepsilon_3 h^{\mathrm{NLOS}}_{qp,f_c}(\tau) \tag{33}$$

where $\varepsilon_1=\sqrt{\frac{\left|h^{\mathrm{B}}_{qp,f_c}(\tau)\right|^2}{\left|h^{\mathrm{B}}_{qp,f_c}(\tau)\right|^2+\left|h^{\mathrm{WR}}_{qp,f_c}(\tau)\right|^2+\left|h^{\mathrm{NLOS}}_{qp,f_c}(\tau)\right|^2}}$, $\varepsilon_2=\sqrt{\frac{\left|h^{\mathrm{WR}}_{qp,f_c}(\tau)\right|^2}{\left|h^{\mathrm{B}}_{qp,f_c}(\tau)\right|^2+\left|h^{\mathrm{WR}}_{qp,f_c}(\tau)\right|^2+\left|h^{\mathrm{NLOS}}_{qp,f_c}(\tau)\right|^2}}$, and $\varepsilon_3=\sqrt{\frac{\left|h^{\mathrm{NLOS}}_{qp,f_c}(\tau)\right|^2}{\left|h^{\mathrm{B}}_{qp,f_c}(\tau)\right|^2+\left|h^{\mathrm{WR}}_{qp,f_c}(\tau)\right|^2+\left|h^{\mathrm{NLOS}}_{qp,f_c}(\tau)\right|^2}}$.

III. Channel Characteristics and System Performance

In Section II, the system model for indoor communication systems is presented. Based on the system model, the vital channel characteristics and channel capacity can be obtained in this section.

A. Channel Transfer Function

Channel transfer function (CTF) is the basis for the analysis of the channel characteristics and performance analysis. Based on [31], the CTFs for the four cases can be obtained, which are the Fourier transform of CIRs.

$$H^{\mathrm{LOS}}_{qp,f_c}(f)=e^{j2\pi(f_c-f)\tau^{\mathrm{L}}_{qp}} \tag{34}$$

$$H^{\mathrm{B}}_{qp,f_c}(f)=\sqrt{T}e^{j2\pi(f_c-f)\tau^{\mathrm{B}}_{qp}} \tag{35}$$

$$H^{\mathrm{WR}}_{qp,f_c}(f)=\sqrt{\Gamma}e^{j2\pi(f_c-f)\tau^{\mathrm{WR}}_{qp}} \tag{36}$$

$$H^{\mathrm{NLOS}}_{qp,f_c}(f)=\sum_{n=1}^{N_{qp}}\sum_{m_n=1}^{M_n}\sqrt{P_{qp,m_n,f_c}}\cdot e^{j2\pi(f_c-f)\tau_{qp,m_n}}. \tag{37}$$

Based on the above expressions, the CTFs for the four cases can be derived as

$$\text{Case 1: } H_{qp,f_c}(f)=\varepsilon_1 H^{\mathrm{LOS}}_{qp,f_c}(f)+\varepsilon_3 H^{\mathrm{NLOS}}_{qp,f_c}(f) \tag{38}$$

$$\text{Case 2: } H_{qp,f_c}(f)=\varepsilon_1 H^{\mathrm{B}}_{qp,f_c}(f)+\varepsilon_3 H^{\mathrm{NLOS}}_{qp,f_c}(f) \tag{39}$$

$$\text{Case 3: } H_{qp,f_c}(f)=\varepsilon_1 H^{\mathrm{LOS}}_{qp,f_c}(f)+\varepsilon_2 H^{\mathrm{WR}}_{qp,f_c}(f)+\varepsilon_3 H^{\mathrm{NLOS}}_{qp,f_c}(f) \tag{40}$$

$$\text{Case 4: } H_{qp,f_c}(f)=\varepsilon_1 H^{\mathrm{B}}_{qp,f_c}(f)+\varepsilon_2 H^{\mathrm{WR}}_{qp,f_c}(f)+\varepsilon_3 H^{\mathrm{NLOS}}_{qp,f_c}(f). \tag{41}$$

B. Spatial Cross-Correlation Function

According to [31], the channel quality can be evaluated by the space non-stationary function which is SCCF. SCCF can measure the effects of MIMO on the channels and describe the correlation between two antennas. SCCFs for the four cases are presented as follows.

1) Case 1: Based on the CTF of Case 1, the SCCF can be obtained by

$$\begin{aligned}&R_{qp,\tilde{p}}\left(f;\Delta r^T\right)=E\left[H_{qp}\left(f\right)H^*_{q\tilde{p}}\left(f\right)\right]\\&=\varepsilon_1^2R^{\mathrm{LOS}}_{qp,\tilde{p}}\left(f;\Delta r^T\right)+\varepsilon_3^2R^{\mathrm{NLOS}}_{qp,\tilde{p}}\left(f;\Delta r^T\right)\\&=\varepsilon_1^2e^{j2\pi\frac{(f_c-f)\left(d_{qp}-d_{q\tilde{p}}\right)}{\lambda f_c}}+\varepsilon_3^2E\left[\sum_{n=1}^{N_{qp}}\sum_{m=1}^{M_n}\sqrt{P_{qp,m_n}\left(f\right)}\right.\\&\left.\sqrt{P_{q\tilde{p},m_n}\left(f\right)}e^{j2\pi\frac{(f_c-f)\left(d_{qp,m_n}-d_{q\tilde{p},m_n}\right)}{\lambda f_c}}\right]\end{aligned} \tag{42}$$

where d_{qp} and $d_{q\tilde{p}}$ can be obtained by (19), d_{qp,m_n} and $d_{q\tilde{p},m_n}$ can be determined by (20).

2) Case 2: The SCCF for Case 2 can be obtained by

$$\begin{aligned}&R_{qp,\tilde{p}}\left(f;\Delta r^T\right)=E\left[H_{qp}\left(f\right)H^*_{q\tilde{p}}\left(f\right)\right]\\&=\varepsilon_1^2R^{\mathrm{B}}_{qp,\tilde{p}}\left(f;\Delta r^T\right)+\varepsilon_3^2R^{\mathrm{NLOS}}_{qp,\tilde{p}}\left(f;\Delta r^T\right)\\&=\varepsilon_1^2Te^{j2\pi\frac{(f_c-f)\left(d_{qp}-d_{q\tilde{p}}\right)}{\lambda f_c}}+\varepsilon_3^2E\left[\sum_{n=1}^{N_{qp}}\sum_{m=1}^{M_n}\sqrt{P_{qp,m_n}\left(f\right)}\right.\\&\left.\sqrt{P_{q\tilde{p},m_n}\left(f\right)}e^{j2\pi\frac{(f_c-f)\left(d_{qp,m_n}-d_{q\tilde{p},m_n}\right)}{\lambda f_c}}\right]\end{aligned} \tag{43}$$

where d_{qp} and $d_{q\tilde{p}}$ can be obtained by (23).

3) Case 3: The SCCF for Case 3 can be obtained by

$$\begin{aligned}
&R_{qp,\tilde{p}}\left(f;\Delta r^T\right)=E\left[H_{qp}\left(f\right)H_{q\tilde{p}}^{*}\left(f\right)\right]\\
&=\varepsilon_1^2R_{qp,\tilde{p}}^{\mathrm{LOS}}\left(f;\Delta r^T\right)+\varepsilon_2^2R_{qp,\tilde{p}}^{\mathrm{WR}}\left(f;\Delta r^T\right)\\
&\quad+\varepsilon_3^2R_{qp,\tilde{p}}^{\mathrm{NLOS}}\left(f;\Delta r^T\right)\\
&=\varepsilon_1^2e^{j2\pi\frac{(f_c-f)\left(d_{qp}-d_{q\tilde{p}}\right)}{\lambda f_c}}+\varepsilon_2^2\Gamma e^{j2\pi\frac{(f_c-f)\left(d_{qp}^{\mathrm{WR}}-d_{q\tilde{p}}^{\mathrm{WR}}\right)}{\lambda f_c}}\\
&\quad+\varepsilon_3^2E\left[\sum_{n=1}^{N_{qp}}\sum_{m=1}^{M_n}\sqrt{P_{qp,m_n}\left(f\right)}\sqrt{P_{q\tilde{p},m_n}\left(f\right)}\right.\\
&\quad\left.e^{j2\pi\frac{(f_c-f)\left(d_{qp,m_n}-d_{q\tilde{p},m_n}\right)}{\lambda f_c}}\right]
\end{aligned}\tag{44}$$

where d_{qp}^{WR} and $d_{q\tilde{p}}^{\mathrm{WR}}$ can be obtained by (28) and the other components are similar to (42).

4) Case 4: The SCCF for Case 4 can be obtained by

$$\begin{aligned}
&R_{qp,\tilde{p}}\left(f;\Delta r^T\right)=E\left[H_{qp}\left(f\right)H_{q\tilde{p}}^{*}\left(f\right)\right]\\
&=\varepsilon_1^2R_{qp,\tilde{p}}^{\mathrm{B}}\left(f;\Delta r^T\right)+\varepsilon_2^2R_{qp,\tilde{p}}^{\mathrm{WR}}\left(f;\Delta r^T\right)\\
&\quad+\varepsilon_3^2R_{qp,\tilde{p}}^{\mathrm{NLOS}}\left(f;\Delta r^T\right)\\
&=\varepsilon_1^2Te^{j2\pi\frac{(f_c-f)\left(d_{qp}-d_{q\tilde{p}}\right)}{\lambda f_c}}+\varepsilon_2^2\Gamma e^{j2\pi\frac{(f_c-f)\left(d_{qp}^{\mathrm{WR}}-d_{q\tilde{p}}^{\mathrm{WR}}\right)}{\lambda f_c}}\\
&\quad+\varepsilon_3^2E\left[\sum_{n=1}^{N_{qp}}\sum_{m=1}^{M_n}\sqrt{P_{qp,m_n}\left(f\right)}\sqrt{P_{q\tilde{p},m_n}\left(f\right)}\right.\\
&\quad\left.e^{j2\pi\frac{(f_c-f)\left(d_{qp,m_n}-d_{q\tilde{p},m_n}\right)}{\lambda f_c}}\right].
\end{aligned}\tag{45}$$

C. Channel Capacity

For the systems with one Tx, channel capacity can be expressed as $C=B\cdot E\left[\log_2(1+\mathrm{SNR})\right]$, where B is the bandwidth and SNR is the signal-to-noise ratio (SNR). According to the approximation derived in [32], it is assumed that $E\left[\log_2(1+\mathrm{SNR})\right]\approx\log_2(1+E[\mathrm{SNR}])$. The expression of $E[\mathrm{SNR}]$ is

$$E[\mathrm{SNR}]=\frac{E\left[\left|\mathbf{H}s\right|^2\right]}{E[|n|^2]}=\frac{E\left[\left|PL^{1/2}\cdot\mathbf{H}_{\mathrm{s}}s\right|^2\right]}{E[|n|^2]}\tag{46}$$

where s means the signal sequence and n is assumed to be the Gaussian white noise. It is assumed that $E[s^2]=P_s$ and $E\left[|n|^2\right]=\sigma_n^2$, where P_s means the signal transmission power and σ_n^2 is the noise power. Then the expression of $E[\mathrm{SNR}]$ can be further derived as

$$E[\mathrm{SNR}]=\frac{PL\cdot P_s}{\sigma_n^2}E\left[\left|\mathbf{H}_{\mathrm{s}}\right|^2\right]\tag{47}$$

where PL can be obtained by (11). The received signal power can be obtained by $PL\cdot P_sE\left[\left|\mathbf{H}_{\mathrm{s}}\right|^2\right]$ and $E\left[\left|\mathbf{H}_{\mathrm{s}}\right|^2\right]$ need to be discussed according to the different cases.

$$E\left[\left|\mathbf{H}_{\mathrm{s}}\right|^2\right]=\sum_{p=1}^{N_T}\sum_{q=1}^{N_R}E\left[H_{qp}\left(f\right)H_{qp}^{*}\left(f\right)\right]\tag{48}$$

Case 1: $E\left[H_{qp}\left(f\right)H_{qp}^{*}\left(f\right)\right]$

$$=\varepsilon_1^2+\varepsilon_3^2E\left[\sum_{n=1}^{N_{qp}}\sum_{m=1}^{M_n}P_{qp,m_n}\left(f\right)\right]\tag{49}$$

Case 2: $E\left[H_{qp}\left(f\right)H_{qp}^{*}\left(f\right)\right]$

$$=\varepsilon_1^2T+\varepsilon_3^2E\left[\sum_{n=1}^{N_{qp}}\sum_{m=1}^{M_n}P_{qp,m_n}\left(f\right)\right]\tag{50}$$

Case 3: $E\left[H_{qp}\left(f\right)H_{qp}^{*}\left(f\right)\right]$

$$=\varepsilon_1^2+\varepsilon_2^2\Gamma+\varepsilon_3^2E\left[\sum_{n=1}^{N_{qp}}\sum_{m=1}^{M_n}P_{qp,m_n}\left(f\right)\right]\tag{51}$$

Case 4: $E\left[H_{qp}\left(f\right)H_{qp}^{*}\left(f\right)\right]$

$$=\varepsilon_1^2T+\varepsilon_2^2\Gamma+\varepsilon_3^2E\left[\sum_{n=1}^{N_{qp}}\sum_{m=1}^{M_n}P_{qp,m_n}\left(f\right)\right].\tag{52}$$

Based on the above derivations, the channel capacity for one-Tx systems can be obtained. However, in the real system, it is difficult to achieve full coverage by one Tx. Hence, multi-Tx systems are necessary although the systems will introduce inter-Tx interference. In the multi-Tx systems, it is assumed that there are M Txs. The i-th Tx could provide the best signal and signals from other Txs can be treated as interference. Then, channel capacity for multi-Tx systems is $C=\sum_{i=1}^{M}B\log_2(1+E[\mathrm{SINR}_i])$ and $E[\mathrm{SINR}_i]$ is

$$E[\mathrm{SINR}_i]=\frac{PL_i\cdot P_{s_i}E\left[\left|\mathbf{H}_{\mathbf{s}_i}\right|^2\right]}{\sum_{j=1,j\neq i}^{M}PL_j\cdot P_{s_j}E\left[\left|\mathbf{H}_{\mathbf{s}_j}\right|^2\right]+\sigma_n^2}\tag{53}$$

where $PL_i, i=1,\ldots,M$ can be obtained by (11) and $E\left[\left|\mathbf{H}_{\mathbf{s}_i}\right|^2\right], i=1,\ldots,M$ can be derived by (48)–(52) depending on the propagation environment between Tx and Rx. Based on the derivations, channel capacity can be obtained.

D. SE and EE

SE can be obtained by the ratio of the channel capacity over the bandwidth. The expression of SE is

$$\mathrm{SE}=\sum_{i=1}^{M}\log_2(1+E[\mathrm{SINR}_i]).\tag{54}$$

EE is another vital KPI, which has raised attentions since 5G. It is measured by the channel capacity provided per joule of energy in bps/J. The expression of EE is $\mathrm{EE}=C/P$ and P is the power consumption. In [33], a power consumption model for indoor wireless communication systems was proposed. The power consumption for indoor Tx can be obtained by

$$P=\frac{P_{\mathrm{BB}}+N_T(P_{\mathrm{RF}}+P_{\mathrm{PA}})}{(1-\eta_{\mathrm{c}})(1-\eta_{\mathrm{ac-dc}})(1-\eta_{\mathrm{dc-dc}})}\tag{55}$$

where $P_{\mathrm{BB/RF/PA}}$ is the power consumption of base band processing/radio frequency front-end/power amplifier and $\eta_{\mathrm{c/ac-dc/dc-dc}}$ is power efficiency of the cooling system/alternating current (AC)-direct current (DC) converters/DC-DC converters. Based on the capacity and power consumption, EE can be calculated.

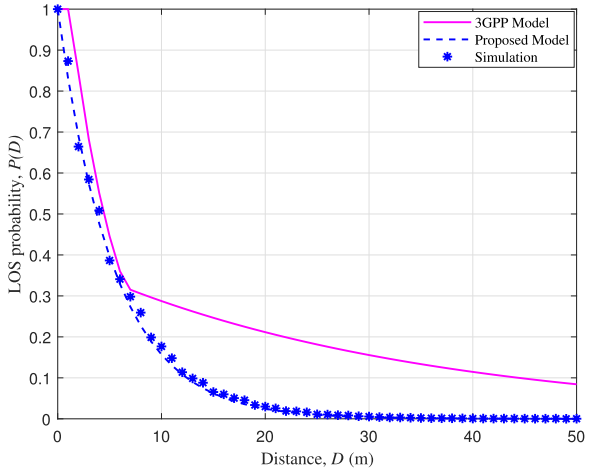

Fig. 5. Comparison between proposed LOS probability model and 3GPP TR 38.901 model ($z_T = 7$ m, $z_R = 1.5$ m, $\sigma = 1.6$ m).

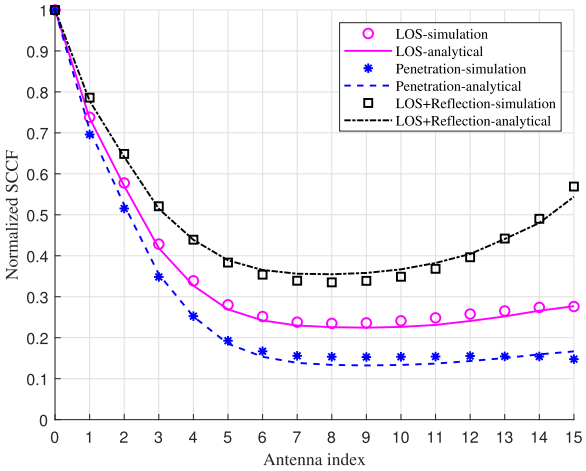

Fig. 6. SCCF considering penetration and reflection ($z_T = 7$ m, $z_R = 1.5$ m, $D = 5\sqrt{2}$ m, $N_T = 16$, $\eta_1 = 1.6$, $\varepsilon = 2.73$).

IV. Results and Analysis

In this section, the theoretical and simulation results are presented and the corresponding analysis is presented. In the simulation, carrier frequency is set as 2.4 GHz. Referring to the size of the factory workshop, the room is set as 50 m $\times$ 50 m $\times$ 7 m. In the room, the blockages include devices, furniture, and walls. The average height and density of devices and furniture is assumed to be 2.5 m and 1 pc/m, respectively. Without loss of generality, the locations of Tx, Rx, and walls are generated randomly, where Txs follow uniform distribution, Rxs and center points of walls follow Poisson point process. The length and orientation of walls are generated randomly. It is assumed that all Txs are deployed on the ceiling and the height of Rx is 1.5 m. Tx is equipped with 16 antennas and Rx is equipped with 4 antennas. In this paper, the values of wall parameters all refer to ITU-R P. 2040-3 [34]. The RDC and the refractive index of wall are assumed to be 2.73 and 1.6, respectively. The other parameters are from [33]. The simulation parameters are set as above, if not otherwise stated later.

Fig. 5 shows the results of LOS probability based on the proposed model and 3GPP TR 38.901 model [8]. When the horizontal projection distance between Tx and Rx is smaller than 7 m, the LOS probability of proposed model and 3GPP model are similar. However, when the distance is larger than 7 m, 3GPP model will overestimate the LOS probability. The results show that when projection distance is larger than 15 m, the received signal can be treated as NLOS signal.

Fig. 6 shows the SCCF considering the penetration and reflection. Comparing the results of Cases 1 and 2, it can be found that penetration reduces the signal power and therefore makes the signal strength weaker, making the SCCF decay faster. The results of Cases 1 and 3 demonstrate that when there is a wall extremely close to the transceiver, the reflected signal approximates the LOS signal, thus enhancing the received signal and reducing the SCCF attenuation rate. The figures validate that the impacts of penetration and reflection are significant.

Fig. 7(a) shows the impacts of penetration and reflection on system performance. As penetration signal suffers from the penetration loss, SE considering penetration is lower than that in LOS scenarios. However, reflected signals are generated by close walls, and due to the proximity of the reflection location, the reflected signals can be regarded as weakened

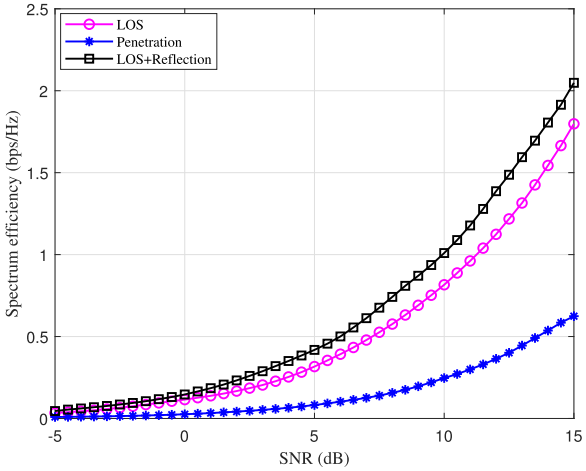

(a) Reflection in LOS scenarios.

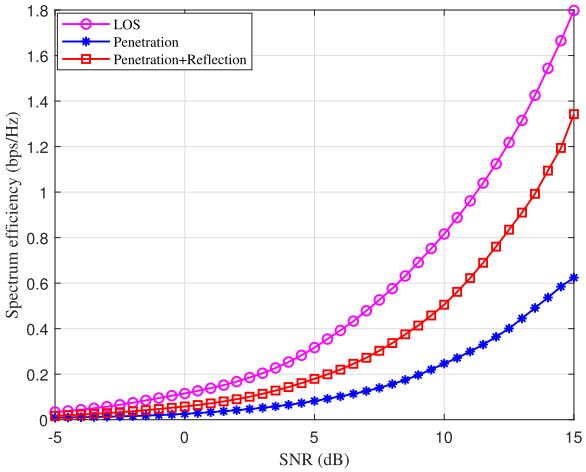

(b) Reflection in penetration scenarios.

Fig. 7. SE considering penetration and reflection ($z_T = 7$ m, $z_R = 1.5$m, $D = 5\sqrt{2}$ m, $N_T = 16$, $N_R = 4$, $\eta_1 = 1.6$, $\varepsilon = 2.73$).

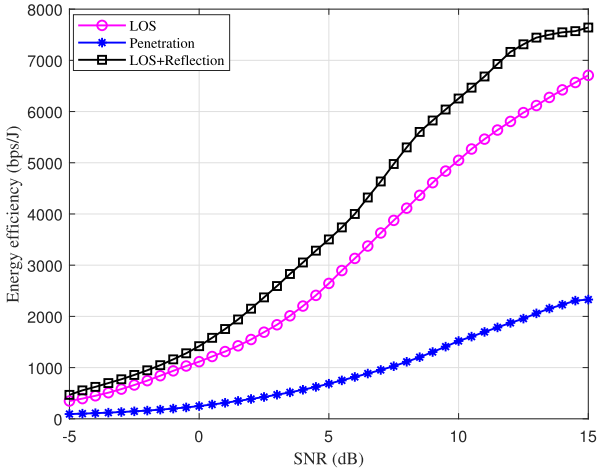

Fig. 8. EE considering the penetration and reflection ($z_T = 7$ m, $z_R = 1.5$ m, $D = 5\sqrt{2}$ m, $N_T = 16, N_R = 4, \eta_1 = 1.6, \varepsilon = 2.73$).

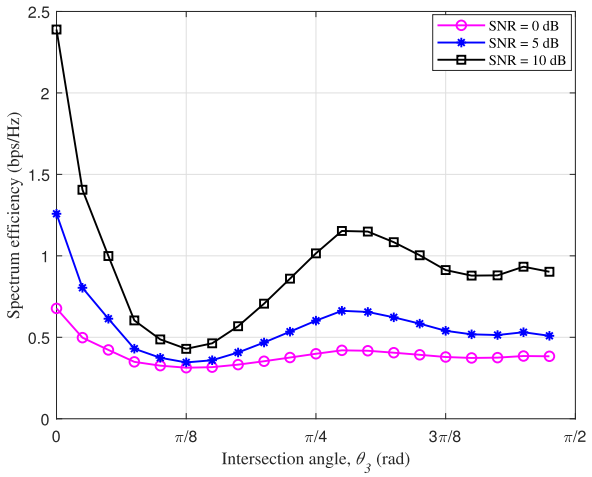

Fig. 9. SE with different intersection angle in penetration scenario ($z_T = 7$ m, $z_R = 1.5$ m, $D = 5\sqrt{2}$ m, $N_T = 16, N_R = 4, \eta_1 = 1.6, \varepsilon = 2.73$).

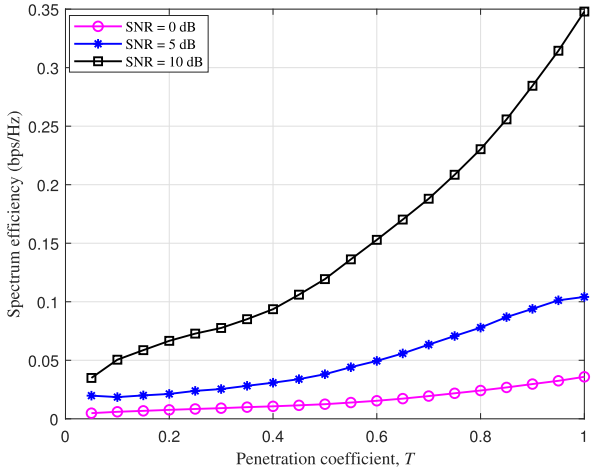

Fig. 10. SE with different penetration coefficient in penetration scenario ($z_T = 7$ m, $z_R = 1.5$ m, $D = 5\sqrt{2}$ m, $N_T = 16, N_R = 4$).

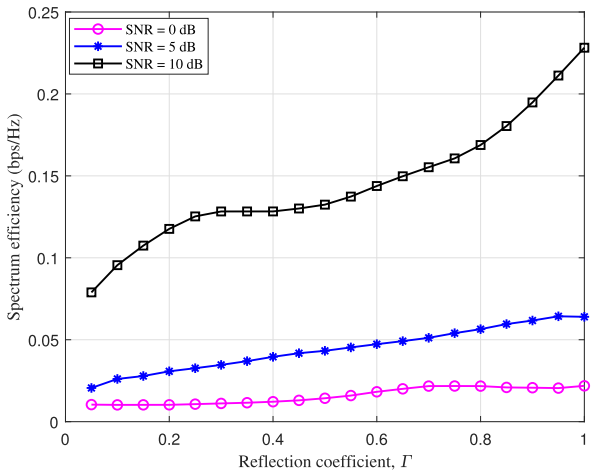

Fig. 11. SE with different reflection coefficient in reflection scenario ($z_T = 7$ m, $z_R = 1.5$ m, $D = 5\sqrt{2}$ m, $N_T = 16, N_R = 4$).

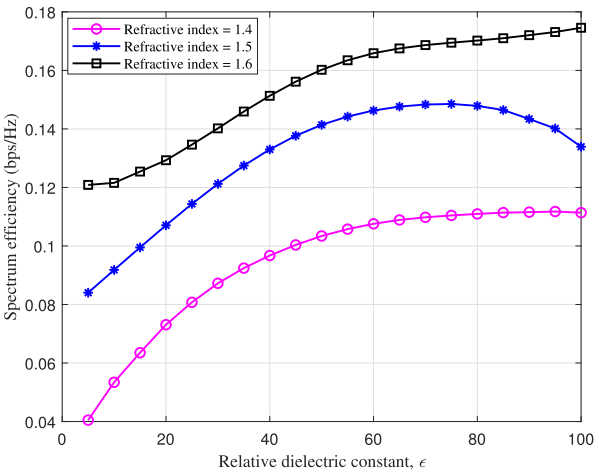

Fig. 12. SE with different RDC considering penetration and reflection ($z_T = 7$ m, $z_R = 1.5$ m, $D = 5\sqrt{2}$ m, $N_T = 16, N_R = 4$).

LOS signals. Therefore, they will enhance the signal quality and thus the SE. As Tx cannot be deployed in each room, penetration is inevitable. Hence, it is possible to introduce reflection to improve the system performance for penetration, which is validated by Fig. 7(b). In Fig. 8, the EE considering penetration and reflection are compared. Walls have a similar effect on EE as SE, with transmission impairing performance and reflection enhancing it. When SNR is higher, EE grows slowly and gradually stabilizes. Since the trends for EE and SE are similar, the later part mainly focuses on SE.

Fig. 9 analyzes SE with different intersection angles under different SNR. When the signal is shot vertically into the wall, the penetrating signal is not refracted, resulting in optimal system performance. However, when vertical incidence is impossible, the intersection angle is optimal around $\pi/4$, and the too large or too small intersection angle will degrade the system performance. Therefore, when the Tx is deployed, the intersection angle should be in the optimal range as much as possible to obtain the optimal system performance.

Fig. 10 and Fig. 11 show the impacts of the penetration and reflection coefficients on SE. For both coefficients, the larger the value, the larger the SE and this gain is further increased as the transmit power of the signal increases. The reason for this is that larger coefficients mean that fewer losses are incurred and therefore performance is improved. However, it is not possible to enhance both the reflection and penetration coefficients for the same material. Therefore, in the design of the communication system, if the wall produces both reflection

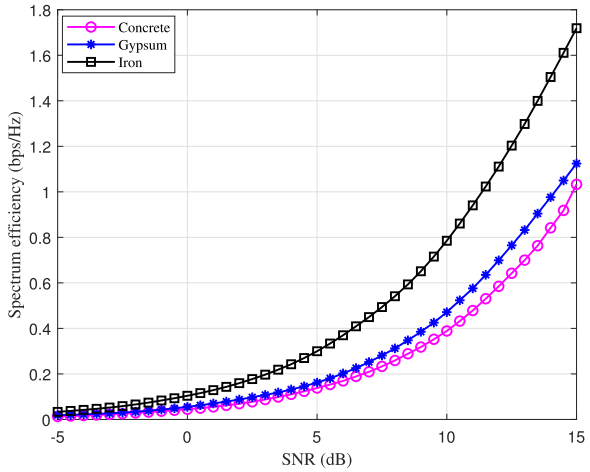

Fig. 13. SE with different wall materials in penetration scenario ($z_T = 7$ m, $z_R = 1.5$ m, $D = 5\sqrt{2}$ m, $N_T = 16$, $N_R = 4$).

and penetration, the two coefficients of the wall material need to be compromised.

Fig. 12 presents SE with different RDC and refractive index. Since common building materials have a refractive index of around 1.5 [34], Fig. 12 illustrates the SE at refractive indices of 1.4, 1.5, and 1.6. As the RDC affects both the penetration and reflection coefficients, optimal performance occurs as the RDC varies. From the graph, it can be seen that when the RDC is too high, there is a tendency for performance to decrease. Therefore, a trade-off between the penetration and reflection coefficients can be achieved through the RDC, which ultimately results in optimal system performance. When RDC is fixed, SE can be improved by adjusting refractive index. Taking concrete, gypsum, and iron as example, Fig. 13 validates that the changes of wall material can further improve system performance.

V. Conclusion

In this paper, the impacts of wall materials and locations on channel characteristics and indoor wireless communication system performance have been investigated. A novel general LOS probability model has been proposed for various indoor wireless communication systems, considering building settings and blockage locations. The average path loss has been derived based on LOS probability. Moreover, indoor propagation links have been divided into four cases considering penetration and reflection of walls and corresponding channel models have been derived. SCCF, channel capacity, SE, and EE have been analyzed. The results have shown that system performance depends on the relative locations between walls and Txs. The SE and EE can be enhanced by setting the intersection angles in a proper range. Moreover, the optimal system performance can be obtained by adjusting RDC to achieve the trade-offs between penetration and reflection coefficients. It is promising to improve the electromagnetic properties of wall materials to ameliorate system performance.

Appendix
Proof of Lemma 1

As shown in Fig. 14, line TU is extended to construct parallelograms RAUV. RA and RV are parallel and equal to

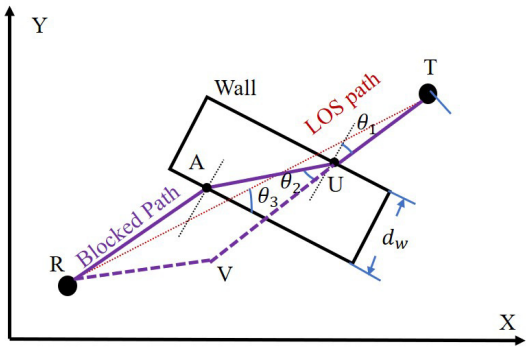

Fig. 14. Derivation for the penetration path in X-Y plane.

UV and UA, respectively. Moreover, $\cos\theta_2 = d_w/\mathrm{AU}$. Based on geometry, it is easy to obtain that $\angle\mathrm{ARV} = \theta_2 - \theta_1$, $\angle\mathrm{ART} = \angle\mathrm{RTU} = \pi/2 - \theta_1 - \theta_3$, $\angle\mathrm{TRV} = \theta_2 + \theta_3 - \pi/2$, and $\angle\mathrm{RVT} = \pi + \theta_1 - \theta_2$. Combining the sine theorem and previous formula, it can be obtained that

$$\begin{cases} \sin\theta_1 = a\sin\theta_2 \\ \cos\theta_2 = d_w/\mathrm{AU} \\ \frac{\cos(\theta_1+\theta_3)}{\mathrm{AU}} = \frac{\sin(\theta_2-\theta_1)}{l} \end{cases} \tag{56}$$

Based on the above equations, a univariate quartic equation can be derived as

$$\begin{aligned} &x^4 + \left(-a^2 - 2l\cos\theta_3\right)x^3 + \left[d_w^2 + 2a^2 l\cos\theta_3 + l^2\cos^2\theta_3 \right. \\ &\left. -(al\sin\theta_3 - d_w)^2\right]x^2 - \left(-2d_w^2 l\cos\theta_3 - a^2 l^2\cos^2\theta_3\right)x \\ &+ d_w^2 l^2\cos^2\theta_3 = 0 \end{aligned} \tag{57}$$

where $x = \sqrt{\mathrm{AU}^2 - d_w^2}$. Let $\xi_1 = 1$, $\xi_2 = -a^2 - 2l\cos\theta_3$, $\xi_3 = d_w^2 + 2a^2 l\cos\theta_3 + l^2\cos^2\theta_3 - (al\sin\theta_3 - d_w)^2$, $\xi_4 = -2d_w^2 l\cos\theta_3 - a^2 l^2\cos^2\theta_3$, $\xi_5 = d_w^2 l^2\cos^2\theta_3$, $\mathcal{D} = 3\xi_2^2 - 8\xi_1\xi_3$, $\mathcal{E} = -\xi_2^3 + 4\xi_1\xi_2\xi_3 - 8\xi_1^2\xi_4$, $\mathcal{F} = 3\xi_2^4 + 16\xi_1^2\xi_3^2 - 16\xi_1\xi_2^2\xi_3 + 16\xi_1^2\xi_2\xi_4 - 64\xi_1^2\xi_5$, $\mathcal{A} = \mathcal{D}^2 - 3\mathcal{F}$, $\mathcal{B} = \mathcal{D}\mathcal{F} - 9\mathcal{E}^2$, $\mathcal{C} = \mathcal{F}^2 - 3\mathcal{D}\mathcal{E}^2$, $\Delta = \mathcal{B}^2 - 4\mathcal{A}\mathcal{C}$, $Z_1 = \mathcal{A}\mathcal{D} + \frac{3\left(-\mathcal{B}+\sqrt{\mathcal{B}^2-4\mathcal{A}\mathcal{C}}\right)}{2}$, $Z_2 = \mathcal{A}\mathcal{D} + \frac{3\left(-\mathcal{B}-\sqrt{\mathcal{B}^2-4\mathcal{A}\mathcal{C}}\right)}{2}$, $\mathcal{G} = \sqrt[3]{Z_1} + \sqrt[3]{Z_2}$, and $Z = \mathcal{D}^2 - \mathcal{D}\mathcal{G} + \mathcal{G}^2 - 3\mathcal{A}$. Then, the solution for x can be obtained by

$$x = \frac{-\xi_2 + \mathrm{sgn}\left(\mathcal{E}\right)\sqrt{\frac{\mathcal{D}+\mathcal{G}}{3}} - \sqrt{\frac{2\mathcal{D}-\mathcal{G}+2\sqrt{Z}}{3}}}{4\xi_1}. \tag{58}$$

As $\mathrm{AU} = \sqrt{x^2 + d_w^2}$, Lemma 1 can be derived.

References

[1] C.-X. Wang et al., "On the road to 6G: Visions, requirements, key technologies and testbeds," *IEEE Commun. Surveys Tuts.*, vol. 25, no. 2, pp. 905–974, 2nd Quart., 2023.

[2] J. Zhang, A. A. Glazunov, W. Yang, and J. Zhang, "Fundamental wireless performance of a building," *IEEE Wireless Commun.*, vol. 29, no. 1, pp. 186–193, Feb. 2022.

[3] *Framework and Overall Objectives of the Future Development of IMT for 2030 and Beyond*, document ITU M.2160, ITU, Nov. 2023. [Online]. Available: https://www.itu.int/rec/R-REC-M.2160/en

[4] Y. Yang, Q. Chu, and C. Mao, "Multiband MIMO antenna for GSM, DCS, and LTE indoor applications," *IEEE Antennas Wireless Propag. Lett.*, vol. 15, pp. 1573–1576, 2016.

[5] S. Chen, J. Zhang, E. Björnson, J. Zhang, and B. Ai, "Structured massive access for scalable cell-free massive MIMO systems," *IEEE J. Sel. Areas Commun.*, vol. 39, no. 4, pp. 1086–1100, Apr. 2021.

[6] X. Pei et al., "RIS-aided wireless communications: Prototyping, adaptive beamforming, and indoor/outdoor field trials," *IEEE Trans. Commun.*, vol. 69, no. 12, pp. 8627–8640, Dec. 2021.

[7] Y. Zhang, J. Zhang, X. Chu, and J. Zhang, "Wireless friendliness evaluation and optimization for sandwich building materials as reflectors," *IEEE Trans. Antennas Propag.*, vol. 72, no. 3, pp. 2697–2711, Mar. 2024.

[8] *Study on Channel Model for Frequencies From 0.5 to 100 GHz*, document TR 38.901, 3GPP, Dec. 2023. [Online]. Available: https://portal.3gpp.org/desktopmodules/Specifications/SpecificationDetails.aspx?specificationId=3173

[9] *Propagation Data and Prediction Methods for the Planning of Indoor Radio Communication Systems and Radio Local Area Networks in the Frequency Range 300 MHz to 450 GHz*, document ITU Rec. P.1238-12, ITU, Aug. 2023. [Online]. Available: https://www.itu.int/rec/R-REC-P.1238

[10] *Propagation Data and Prediction Methods Required for the Design of Terrestrial Broadband Radio Access Systems Operating in a Frequency Range From 3 GHz to 60 GHz*, document ITU Rec. P.1410-6, ITU, Aug. 2023. [Online]. Available: https://www.itu.int/rec/R-REC-P.1410/en

[11] M. K. Elmezughi and T. J. Afullo, "Evaluation of line-of-sight probability models for enclosed indoor environments at 14 to 22 GHz," in *Proc. Int. Conf. Artif. Intell., Big Data, Comput. Data Commun. Syst. (icABCD)*, Aug. 2021, pp. 1–6.

[12] W. Yang, J. Zhang, A. A. Glazunov, and J. Zhang, "Line-of-sight probability for channel modeling in 3-D indoor environments," *IEEE Antennas Wireless Propag. Lett.*, vol. 19, no. 7, pp. 1182–1186, Jul. 2020.

[13] M. Nemati, B. Maham, S. R. Pokhrel, and J. Choi, "Modeling RIS empowered outdoor-to-indoor communication in mmWave cellular networks," *IEEE Trans. Commun.*, vol. 69, no. 11, pp. 7837–7850, Nov. 2021.

[14] Y. Wu, J. Kokkoniemi, C. Han, and M. Juntti, "Interference and coverage analysis for terahertz networks with indoor blockage effects and line-of-sight access point association," *IEEE Trans. Wireless Commun.*, vol. 20, no. 3, pp. 1472–1486, Mar. 2021.

[15] I. Cuinas and M. G. Sanchez, "Measuring, modeling, and characterizing of indoor radio channel at 5.8 GHz," *IEEE Trans. Veh. Technol.*, vol. 50, no. 2, pp. 526–535, Mar. 2001.

[16] Y. Liu, J. Zhang, Y. Zhang, Z. Yuan, and G. Liu, "A shared cluster-based stochastic channel model for integrated sensing and communication systems," *IEEE Trans. Veh. Technol.*, vol. 73, no. 5, pp. 6032–6044, May 2024.

[17] P. Tennakoon and C. B. Wavegedara, "A GBSM indoor channel model with an arbitrary center point of Gaussian scatterer distribution," *IEEE Trans. Antennas Propag.*, vol. 70, no. 3, pp. 2128–2136, Mar. 2022.

[18] M. Jacob, S. Priebe, R. Dickhoff, T. Kleine-Ostmann, T. Schrader, and T. Kurner, "Diffraction in mm and sub-mm wave indoor propagation channels," *IEEE Trans. Microw. Theory Techn.*, vol. 60, no. 3, pp. 833–844, Mar. 2012.

[19] L. Zhang et al., "Multifrequency wireless channel measurements and characterization in large indoor office environments," *IEEE Trans. Antennas Propag.*, vol. 71, no. 6, pp. 5221–5234, Jun. 2023.

[20] C.-X. Wang, Z. Lv, X. Gao, X. You, Y. Hao, and H. Haas, "Pervasive wireless channel modeling theory and applications to 6G GBSMs for all frequency bands and all scenarios," *IEEE Trans. Veh. Technol.*, vol. 71, no. 9, pp. 9159–9173, Sep. 2022.

[21] M. K. Müller, M. Taranetz, and M. Rupp, "Effects of wall-angle distributions in indoor wireless communications," in *Proc. IEEE 17th Int. Workshop Signal Process. Adv. Wireless Commun. (SPAWC)*, Jul. 2016, pp. 1–5.

[22] K. Venugopal and R. W. Heath, "Millimeter wave networked wearables in dense indoor environments," *IEEE Access*, vol. 4, pp. 1205–1221, 2016.

[23] Z. Yun and M. F. Iskander, "UWB pulse propagation through complex walls in indoor wireless communications environments," in *Proc. Int. Conf. Wireless Netw., Commun. Mobile Comput.*, vol. 2, Dec. 2005, pp. 1358–1361.

[24] Z. Yun, M. F. Iskander, and Z. Zhang, "Complex-wall effect on propagation characteristics and MIMO capacities for an indoor wireless communication environment," *IEEE Trans. Antennas Propag.*, vol. 52, no. 4, pp. 914–922, Apr. 2004.

[25] M. Dong, Y. Qi, X. Wang, and Y. Liu, "A non-line-of-sight mitigation method for indoor ultra-wideband localization with multiple walls," *IEEE Trans. Ind. Informat.*, vol. 19, no. 7, pp. 8183–8195, Jul. 2023.

[26] J. Zhang, A. A. Glazunov, and J. Zhang, "Wireless performance evaluation of building layouts: Closed-form computation of figures of merit," *IEEE Trans. Commun.*, vol. 69, no. 7, pp. 4890–4906, Jul. 2021.

[27] Y. Zhang, C. Chen, S. Yang, J. Zhang, X. Chu, and J. Zhang, "How friendly are building materials as reflectors to indoor LOS MIMO communications?," *IEEE Internet Things J.*, vol. 7, no. 9, pp. 9116–9127, Sep. 2020.

[28] Z. Li, H. Hu, J. Zhang, and J. Zhang, "Impact of wall penetration loss on indoor wireless networks," *IEEE Antennas Wireless Propag. Lett.*, vol. 20, no. 10, pp. 1888–1892, Oct. 2021.

[29] S. Roy and M. Mehrnoush, "A new Poisson process-based model for LOS/NLOS discrimination in clutter modeling," *IEEE Trans. Antennas Propag.*, vol. 67, no. 12, pp. 7538–7549, Dec. 2019.

[30] M. Born and E. Wolf, *Principles of Optics: Electromagnetic Theory of Propagation, Interference and Diffraction of Light*. Cambridge, U.K.: Cambridge Univ. Press, 1999.

[31] C.-X. Wang, Z. Lv, Y. Chen, and H. Haas, "A complete study of space-time-frequency statistical properties of the 6G pervasive channel model," *IEEE Trans. Commun.*, vol. 71, no. 12, pp. 7273–7287, Dec. 2023.

[32] Q. Zhang, S. Jin, K.-K. Wong, H. Zhu, and M. Matthaiou, "Power scaling of uplink massive MIMO systems with arbitrary-rank channel means," *IEEE J. Sel. Topics Signal Process.*, vol. 8, no. 5, pp. 966–981, Oct. 2014.

[33] Y. Fu, C.-X. Wang, X. Mao, J. Huang, Z. Zhao, and S. McLaughlin, "Spectrum-energy-economy efficiency analysis of B5G wireless communication systems with separated indoor/outdoor scenarios," *IEEE Trans. Wireless Commun.*, vol. 22, no. 12, pp. 9718–9731, Dec. 2023.

[34] *Effects of Building Materials and Structures on Radiowave Propagation Above About 100 MHz*, document ITU-R P. 2040-3, ITU, Aug. 2023. [Online]. Available: https://www.itu.int/rec/R-REC-P.2040/en

Xichen Mao (Graduate Student Member, IEEE) received the B.E. degree in communication engineering from Jilin University, China, in 2021. He is currently pursuing the Ph.D. degree with the National Mobile Communications Research Laboratory, Southeast University, China. He is also a Visiting Ph.D. Student with the School of Electrical Engineering and Telecommunications, University of New South Wales, Australia, supported by China Scholarship Council. His research interests include performance analysis and optimization for 6G indoor wireless communication systems.

Cheng-Xiang Wang (Fellow, IEEE) received the B.Sc. and M.Eng. degrees in communication and information systems from Shandong University, Jinan, China, in 1997 and 2000, respectively, and the Ph.D. degree in wireless communications from Aalborg University, Aalborg, Denmark, in 2004.

He was a Research Assistant with Hamburg University of Technology, Hamburg, Germany, from 2000 to 2001; a Visiting Researcher with Siemens AG Mobile Phones, Munich, Germany, in 2004; and a Research Fellow with the University of Agder, Grimstad, Norway, from 2001 to 2005. He was with Heriot-Watt University, Edinburgh, U.K., from 2005 to 2018, where he was promoted to a Professor in 2011. Since 2018, he has been with Southeast University, Nanjing, China, as a Professor, where he is currently the Dean of the School of Information Science and Engineering. He is also a Professor with the Pervasive Communication Research Center, Purple Mountain Laboratories, Nanjing. He has authored four books, three book chapters, and more than 660 refereed journal articles and conference proceedings, including 31 highly-cited papers. His current research interests include wireless channel measurements and modeling, 6G wireless communication networks, and electromagnetic information theory.

Dr. Wang is a member of the Academia Europaea (The Academy of Europe), a member of European Academy of Sciences and Arts (EASA), a fellow of the Royal Society of Edinburgh (FRSE) and IET, an IEEE Communications Society Distinguished Lecturer in 2019 and 2020, and a Highly-Cited Researcher recognized by Clarivate Analytics. He is currently an Executive Editorial Committee Member of IEEE TRANSACTIONS ON WIRELESS COMMUNICATIONS. He has served as an Editor for more than 16 international journals, including IEEE TRANSACTIONS ON WIRELESS COMMUNICATIONS from 2007 to 2009, IEEE TRANSACTIONS ON VEHICULAR TECHNOLOGY from 2011 to 2017, and IEEE TRANSACTIONS ON COMMUNICATIONS from 2015 to 2017. He was a Guest Editor of IEEE JOURNAL ON SELECTED AREAS IN COMMUNICATIONS, IEEE TRANSACTIONS ON BIG DATA, and IEEE TRANSACTIONS ON COGNITIVE COMMUNICATIONS AND NETWORKING. He has served as the TPC chair and the general chair for more than 30 international conferences. He received the IEEE Neal Shepherd Memorial Best Propagation Paper Award in 2024. He also received 19 Best Paper Awards from international conferences. He has also delivered 39 invited keynote speeches/talks and 23 tutorials at international conferences.

Songjiang Yang (Member, IEEE) received the B.Eng. (Hons.) and Ph.D. degrees in electrical and electronic engineering from the University of Sheffield, Sheffield, U.K., in 2017 and 2022, respectively. He is currently a Post-Doctoral Researcher at the Pervasive Communication Research Center, Purple Mountain Laboratories, Nanjing, China. His current research interests include ray-tracing channel modeling, UAV communications, and system performance evaluation. He was selected for the Outstanding Postdoctoral Fellow Program in Jiangsu Province and received the Best Paper Award from WCSP 2024, IEEE ICCT 2025, and CIoTSC 2025.

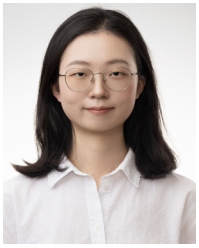

Jingyu Lyu received the B.E. degree in information engineering and the M.E. degree in information and communication engineering from Southeast University, China, in 2022 and 2025, respectively. Her research interests include ray-tracing channel modeling and network planning.

Jie Huang (Member, IEEE) received the B.E. degree in information engineering from Xidian University, China, in 2013, and the Ph.D. degree in information and communication engineering from Shandong University, China, in 2018. From October 2018 to October 2020, he was a Post-Doctoral Research Associate with the National Mobile Communications Research Laboratory, Southeast University, China, supported by the National Postdoctoral Program for Innovative Talents. From January 2019 to February 2020, he was a Post-Doctoral Research Associate with Durham University, U.K. Since March 2019, he has been a part-time Researcher with Purple Mountain Laboratories, China. Since November 2020, he has been an Associate Professor with the National Mobile Communications Research Laboratory, Southeast University. He has authored and co-authored more than 160 papers in refereed journals and conference proceedings. His research interests include millimeter wave, massive MIMO, reconfigurable intelligent surface channel measurements and modeling, electromagnetic information theory, and 6G wireless communications. He received the IEEE Neal Shepherd Memorial Best Propagation Paper Award in 2024 and the Best Paper Awards from WPMC 2016, WCSP 2020, WCSP 2021, WCSP 2024, and IEEE ICCT 2025. He has served as an Editor for IEEE TRANSACTIONS ON GREEN COMMUNICATIONS AND NETWORKING and an Associate Editor for IEEE TRANSACTIONS ON VEHICULAR TECHNOLOGY. He has delivered more than 15 tutorials in international conferences, including IEEE Globecom and IEEE ICC.

Shuaifei Chen (Member, IEEE) received the B.S. degree in communication engineering and the Ph.D. degree in information and communication engineering from Beijing Jiaotong University, China, in 2018 and 2023, respectively.

From 2019 to 2020, he visited the Department of Communication Systems, Linköping University, Sweden. From 2021 to 2022, he visited the Division of Communication Systems, KTH Royal Institute of Technology, Sweden. He is currently a Research Associate Professor with the Pervasive Communication Research Center, Purple Mountain Laboratories, Nanjing, China, and a Post-Doctoral Researcher with the National Mobile Communications Research Laboratory, School of Information Science and Engineering, Southeast University, Nanjing. Since January 2025, he has been an External Supervisor with Southeast University. His research interests include signal processing and resource allocation for wireless communications, cell-free massive MIMO, and digital twin-aided 6G multiple antenna technologies. He serves as a Technical Program Committee (TPC) Member for several conferences, including IEEE ICC and IEEE PIMRC. He was a recipient of the Best Paper Award from IEEE ICC 2025. He was selected in the Outstanding Postdoctoral Fellow Program in Jiangsu in 2024 and the Young Elite Scientists Sponsorship Program by Jiangsu Association for Science and Technology (JSAST) in 2025. He was recognized as an Exemplary Reviewer of IEEE TRANSACTIONS ON COMMUNICATIONS in 2021 and IEEE COMMUNICATIONS LETTERS in 2023.

Jie Zhang (Senior Member, IEEE) received the Ph.D. degree in industrial automation from East China University of Science and Technology, Shanghai, China, in 1995. Since January 2011, he has been the Chair of Wireless Systems with the Department of Electronic and Electrical Engineering, University of Sheffield, Sheffield, U.K., on a part-time basis. Prior to joining the University of Sheffield, he had studied/worked with Imperial College London, Oxford University, and the University of Bedfordshire, reaching the status of a Senior Lecturer, a Reader, and a Professor in 2002, 2005, and 2006, respectively. He is also the Founder, the Board Director, and the Chief Scientific Officer at Ranplan Wireless Network Design Ltd., Cambridge, U.K., a public company listed on Nasdaq First North. Ranplan Wireless produces a suite of world-leading indoor and the first joint indoor-outdoor radio access network planning tools–Ranplan Professional, which is being used by all the top five telecom equipment vendors and the world's largest mobile operators, system integrators, and research organizations. Along with his students and colleagues, he has pioneered research in small cell and heterogeneous networks and published some of the landmark papers and books on these topics, widely used by both academia and industry. Since 2010, he and his team have also developed ground-breaking work in smart radio environment and building wireless performance modeling, evaluation, and optimization, the key concepts of which were introduced in a paper titled "Fundamental Wireless Performance of a Building," IEEE WIRELESS COMMUNICATIONS, 29(1), 2022. His Google Scholar citations are in excess of 8500 with an H-index of 40.